Magnesium Technology 2015
Edited by: Michele V. Manuel, Alok Singh, Martyn Alderman, and Neale R. Neelameggham
TMS (The Minerals, Metals & Materials Society), 2015

SIMULATION OF CONCURRENT PRECIPITATION OF TWO STRENGTHENING PHASES IN MAGNESIUM ALLOYS

Weihua Sun[1], Chuan Zhang[2], Andrew D. Klarner[1], Weisheng Cao[2], Alan A. Luo[1, 3]
[1]Department of Materials Science and Engineering, The Ohio State University, Columbus, OH 43210, USA
[2]CompuTherm LLC, Madison, WI 53719, USA
[3]Department of Integrated Systems Engineering, The Ohio State University, Columbus, OH 43210, USA

Keywords: Magnesium alloys, Precipitation simulation, CALPHAD

Abstract

The precipitation kinetics and microstructure in Mg-Sn binary and Mg-Al-Sn ternary alloys are simulated using PanPrecipitation coupled with Mg thermodynamic database and a newly established mobility database of the Mg-Al-Sn ternary system. Both Mg_2Sn and $Mg_{17}Al_{12}$ precipitates are considered in this work. The obtained kinetic parameters for these two precipitates can be used in the simulation of both individual and concurrent precipitations of $Mg_{17}Al_{12}$ and Mg_2Sn in Mg-Al-Sn alloys. The simulated microstructure evolution, such as the particle size and number density, are in agreement with experimental data.

Introduction

Magnesium alloys are considered as promising lightweight materials in the transportation industry due to their low density. Currently, the most widely used Mg alloys in industry are Mg-Al based alloys, but their usage is limited to room temperature applications because of their poor creep resistance at elevated temperatures. The poor performance of current Mg-Al based alloys at temperature above 120°C is caused by the softening of grain boundary $Mg_{17}Al_{12}$, which has a low melting point of 450°C [1]. Luo et al. [2] systematically investigated the microstructure and mechanical properties of as-cast Mg-Al-Sn alloys and suggested that Mg-7Al-2Sn and Mg-7Al-5Sn (wt.%) offer good balance of mechanical properties. The Mg-Al-Sn system consists of two aging hardening systems, i.e., Mg-Al and Mg-Sn systems. By precipitation of fine $Mg_{17}Al_{12}$ and/or Mg_2Sn particles in (Mg) matrix during aging, the yield strength of Mg-Al-Sn alloys could be improved, as reported from the investigation of Mg-7Al-2Sn (wt.%) alloy by Shi et al. [3]. Moreover, the precipitation of Mg_2Sn with a melting point of 774°C could improve the creep resistance of the alloys at elevated temperatures [4].

In order to develop precipitation hardening in Mg-Al-Sn alloys, both experimental and simulation work should be carried out to understand the microstructure evolution during aging process and its influence on the mechanical properties of the alloys. Previously, Zhang et al. [5] has simulated the precipitation of AZ91 alloy during aging process with PanPrecipitation of Pandat software [6]. In the present work, previous work on AZ91 alloy [5] will be extended to simulate the precipitation of Mg_2Sn in Mg-Sn binary alloys and concurrent precipitation of $Mg_{17}Al_{12}$ and Mg_2Sn in Mg-Al-Sn ternary alloys during aging. The microstructure evolution information, such as number density, average particle size etc., will be predicted.

Methodology

The general flowchart of precipitation simulation is shown in Fig. 1. In order to perform a quantitative simulation, reliable thermodynamic and mobility databases for Mg-Al-Sn system should be available for extracting accurate thermodynamic and mobility data, such as driving force and diffusivity. In the present simulation, the PanMagnesium thermodynamic database [7] is directly utilized. The atomic mobility database of Mg-Al-Sn system is developed in this study based on assessment of diffusion data in literature using the CALPHAD approach (CALculation of PHAse Diagrams) [8] as a first step. The parameters including nucleation site parameter and interfacial energy of Mg_2Sn/(Mg) are then calibrated from the simulation of the two Mg-Sn alloys in this study. The simulated microstructure evolution information, such as number density and size of precipitate will be compared with experimental data in literature. Finally, by combing the parameters for Mg_2Sn/Mg in the current work and the modified parameters for $Mg_{17}Al_{12}$/Mg based on previous work [5], the concurrent precipitation of two precipitates in Mg-Al-Sn alloys is predicted. The basic theories for atomic mobility assessment and precipitation simulation are briefly introduced as follows.

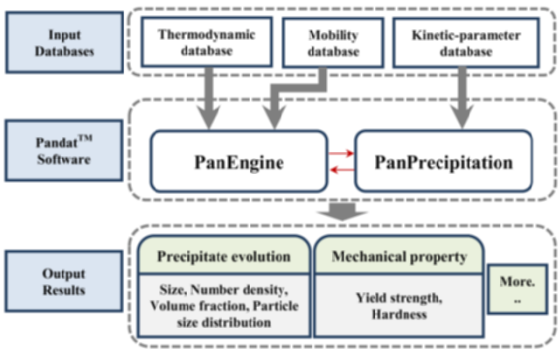

Figure 1. The architecture of PanPrecipitation [5]

Atomic mobility assessment

According to the absolute rate theory arguments, the atomic mobility of the element B, M_B can be divided into a frequency factor M_B^0 and an activation enthalpy Q_B [9, 10]. M_B can be expressed as [9]:

$$M_B = M_B^0 \exp\left(\frac{-Q_B}{RT}\right)\frac{1}{RT} = \exp\left(\frac{RT\ln M_B^0}{RT}\right)\exp\left(\frac{-Q_B}{RT}\right)\frac{1}{RT} \qquad (1)$$

Where R is the gas constant and T is the temperature. The parameters $RT\ln M_B^0$ and Q_B are dependent on temperature, composition and pressure. In CALPHAD approach, the composition dependency of these two parameters can be expressed by a linear combination of the values at each endpoint

of the composition space and a Redlich-Kister polynomial [11]:

$$\Phi_B = \sum_i x_i \Phi_B^i + \sum_i \sum_{j>i} x_i x_j \left[\sum_{r=0}^{m} {}^r\Phi_B^{i,j}(x_i - x_j)^r\right] + \sum_i \sum_{j>i} \sum_{k>j} x_i x_j x_k \left[\sum_s v_{ijk}^s {}^s\Phi_B^{i,j,k}\right] \quad (s = i, j, k) \quad (2)$$

Where x_i is the molar fraction of element i, Φ_B^i is for pure i and represents the value of one endpoint in the composition space. ${}^r\Phi_B^{i,j}$ and ${}^s\Phi_B^{i,j,k}$ are the binary and ternary interaction parameters. The parameter v_{ijk}^s is given by

$$v_{ijk}^s = x_s + (1 - x_i - x_j - x_k)/3 \quad (s = i, j \text{ or } k) \quad (3)$$

Assuming the monovacancy atomic exchange as the main diffusion mechanism, the tracer diffusivity D_i^* is related to the atomic mobility M_i by the Einstein's relation:

$$D_i^* = RTM_i \quad (4)$$

For a substitutional solution phase, the interdiffusion coefficient in terms of the volume fixed reference frame can be given by the following expression:

$$\tilde{D}_{kj}^n = \sum_i (\delta_{ik} - x_k) \cdot x_i \cdot M_i \cdot \left(\frac{\partial \mu_i}{\partial x_j} - \frac{\partial \mu_i}{\partial x_n}\right) \quad (5)$$

Where δ_{ik} is the Kronecker delta (δ_{ik}=1 if i=k, otherwise δ_{ik}=0), μ_i is the chemical potential. Based on the relations above, the parameter Φ_B can be numerically assessed by fitting to the experimental diffusion coefficients including self diffusivity, tracer diffusivity and chemical diffusivity.

Precipitation simulation

The classical precipitation model KWN (Kampmann-Wagner-numerical) model [12] implemented in PanPrecipitation is selected for the current work. This model features the capability of modeling nucleation, growth and coarsening simultaneously. The precipitates are divided into a series of size classes. At each time step, the microstructure information in each size class is updated taking into account of the concurrence of nucleation, growth and coarsening. The matrix composition is updated according to the mass conservation equation at the end of each step. This model generally consists of three equations. The nucleation rate is calculated by the classic nucleation theory:

$$J = N_0 Z\beta \exp\left(-\frac{\Delta G^*}{kT}\right)\exp\left(-\frac{\tau}{t}\right) \quad (6)$$

N_0 is the nucleation site density, *Z* is the Zeldovich factor and β is the rate at which the atoms from the matrix are attached to the critical nucleus. ΔG* is the Gibbs energy of formation of a critical nucleus. k is the Boltzmann constant, T is the temperature. τ is the incubation time for nucleation, t is the time.

The growth of precipitates is expressed by a model proposed by Morral and Purdy [13]. This model for multicomponent alloys assumes a diffusion-controlled process and takes into account the Gibbs-Thomson effect.

$$\frac{dR}{dt} = \frac{K}{R}\left(\frac{1}{R^*} - \frac{1}{R}\right) \quad (7)$$

$$K = \frac{2\alpha V_m}{(C^{\alpha\beta})[M]^{-1}[C^{\alpha\beta}]} \quad (8)$$

R is the radius of the interface and R* is the radius of the critical nucleus. V_m is the molar volume of the precipitate. ($C^{\alpha\beta}$] and [$C^{\alpha\beta}$) are the row and column vector of the solute concentration difference between matrix phase and precipitate. [M] is the chemical mobility matrix. The flux of precipitates in and out the each size is expressed by the following continuity equation:

$$\frac{\partial N(r,t)}{\partial t} = -\frac{\partial (N(r,t)v(r,t)}{\partial r} + \delta(r - r_{cr}(t))j(t) \quad (9)$$

N(r,t) is the number density of precipitate and v(r,t) is the growth velocity. δ is the Kronecker delta. r_{cr} is the critical radius.

Results and discussion

Atomic mobility assessment

There are just a few experimental diffusion coefficients related to the hcp(Mg) phase of Mg-Al-Sn system, as listed in Table I. It can be seen from Fig. 2 that there is discrepancy among the experimental interdiffusion coefficients from Ref. [19-21]. The data reported by Kulkarni and Luo [21] are less concentration dependent and more self-consistent, while the data from Kammerer et al. [19] and Brennan et al. [20] are more concentration dependent. More diffusion experiment is needed to clarify the discrepancy.

Table I. Summary of experimental data for hcp (Mg) of Mg-Al-Sn alloys.

System	Date Type		Temp. range(K)	Ref.
Mg	Self diffusion	D_{Mg}^{Mg}	741-908 775-906	[14] [15]
Mg-Al	Impurity diffusion	D_{Al}^{Mg}	573-673 635-693 623-723	[16] [17] [18]
	Inter-diffusion	D_{AlAl}^{Mg}	623-723 573-673 653-693	[19] [20] [21]
Mg-Sn	Impurity diffusion	D_{Sn}^{Mg}	748-903	[22]

The atomic mobility parameters are listed in Table II and only the parameters of nine end members are used without introduction of any binary or ternary interaction parameter. The Q_{Mg}^{Mg} is directly obtained from experimental self diffusion coefficient of Mg [15]. Q_{Sn}^{Mg} is from experimental impurity diffusion coefficient of Sn in hcp(Mg) [22] because no other data are reported. Since the impurity diffusion coefficients of Al in hcp(Mg) from Brennan et al. [16] are in agreement with the data from Das et al. [17], their data [16] are used for Q_{Al}^{Mg}. It should be mentioned that no interaction parameter is introduced for Mg-Al system since in the optimization process, the atomic mobility of Mg-Al system consisted of only four end member parameters could describe the interdiffusion coefficient of Ref. [21] , as shown in Fig. 2. The introduction of interaction parameters has no significant improvement of the fitting to the experimental data. The hypothetical end member parameter Q_{Al}^{Al} is from the estimation of Cui et al. [23]. Q_{Sn}^{Sn} is estimated using the empirical equation [24].

$$Q_B = RT_m(K + 1.5V) \quad (10)$$

$$D_0 = 2.506 \times 10^9 Q_B a^2 \quad (11)$$

Q_B is the activation energy and D_0 is the frequency factor. K denotes the crystal structure factor, V is the valence, and a is the lattice constant. For metastable Sn with hcp structure, the melting point is calculated to be 499K [7], K=15.5 for hcp phase [24], V=2.5 [24], a=3.282Å [25], so Q_{Sn}=79862 J/mol and D_0=2.15576×10^{-5}m^2/s. The other hypothetical end members Q^{Sn}_{Mg} and Q^{Sn}_{Al} are assumed to be equal to the mobility parameter Q^{Sn}_{Sn} while Q^{Al}_{Mg} and Q^{Al}_{Sn} are equal to Q^{Al}_{Al}.

Table II Summary of the atomic mobility for Mg, Al and Sn in hcp(Mg) of the Mg-Al-Sn system assessed in the present work.

Mobility	Parameter
Mg	$Q^{Mg}_{Mg} = -138164 + R*T*LN(1.75E-4)$ $Q^{Al}_{Mg} = -79790 + R*T*LN(2.38E-5)$ $Q^{Sn}_{Mg} = -79862 + R*T*LN(2.15576E-5)$
Al	$Q^{Mg}_{Al} = -155000 + R*T*LN(3.9E-3)$ $Q^{Al}_{Al} = -79790 + R*T*LN(2.38E-5)$[a] $Q^{Sn}_{Al} = -79862 + R*T*LN(2.15576E-5)$
Sn	$Q^{Mg}_{Sn} = -149887 + R*T*LN(4.8251E-4)$ $Q^{Al}_{Sn} = -79790 + R*T*LN(2.38E-5)$ $Q^{Sn}_{Sn} = -79862 + R*T*LN(2.15576E-5)$

[a]: From assessment by Cui et al. [23]

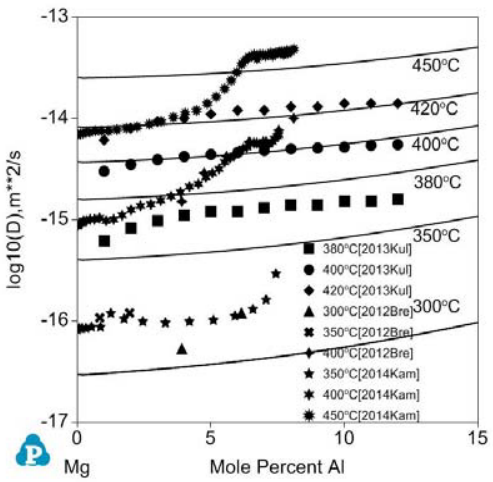

Figure 2. Calculated interdiffusion coefficients in the Mg rich region of Mg-Al system along with the experimental data from Ref. [19-21].

Precipitation simulation

The shape of Mg_2Sn precipitate is not spherical according to the experimental observations [26]. By assuming shape-preserved growth of the precipitate, the shape of the precipitate could be treated as sphere [5]. The conversion method described by Zhang et al. [5] is used to calculate the equivalent particle size. By coupling to the thermodynamic database and the atomic mobility parameters described above, the precipitation of Mg_2Sn at 200°C in two supersaturated Mg-Sn alloys is simulated in the first step. Figure 3 shows the calculated number density for the two Mg-Sn alloys are in agreement with the experimental data [26]. Figure 4 shows the predicted radius for Mg-1.9 at.% Sn alloy at 240 hours is 128nm, which is consistent with the experimental value of 112nm [26]. However, for the Mg-1.3 at.% Sn alloy, the simulated radius at 1000 hours is 160nm, which is lower than the experimental value of 197 nm [26], but still within the experimental error range. Table III shows the parameters used for the simulation. The nucleation site parameter and interfacial energy are two adjustable parameters in the simulation.

Table III Parameters used in the simulation.

Parameter	Value
Nucleation site parameter	1×10^{-14}
Interfacial energy of Mg/Mg_2Sn interface	0.25 J/m^2
Molar volume of hcp(Mg) matrix	1.4×10^{-5}m^3/mol
Molar volume of Mg_2Sn precipitate	1.55×10^{-5}m^3/mol

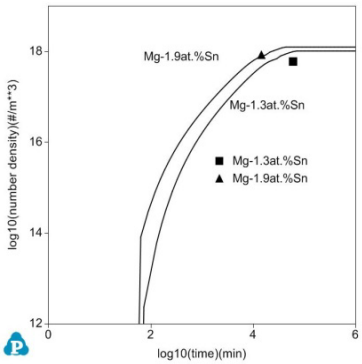

Figure 3. Predicted number density of Mg_2Sn precipitate in Mg-1.3 at.% Sn and Mg-1.9 at.% alloys along with the experimental data [26].

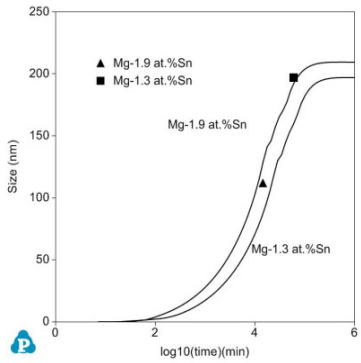

Figure 4. Predicted radius of Mg_2Sn precipitate in Mg-1.3 at.% Sn and Mg-1.9 at.% alloys along with the experimental data [26].

By combining the parameters for Mg_2Sn and $Mg_{17}Al_{12}$, the concurrent precipitation of $Mg_{17}Al_{12}$ and Mg_2Sn at 200°C in Mg-7Al-2Sn (wt.%) alloy is simulated. Figure 5 shows the volume fractions of of Mg_2Sn and $Mg_{17}Al_{12}$. After about 100 hours, the fraction of $Mg_{17}Al_{12}$ reaches equilibrium value while the fraction of Mg_2Sn is considerably low. There are two reasons, the nucleation of $Mg_{17}Al_{12}$ is considerably stronger than that of Mg_2Sn as shown in Fig. 6 and the growth of $Mg_{17}Al_{12}$ is faster as can be seen in Fig.7. According to the simulation, the precipitation of $Mg_{17}Al_{12}$ is much stronger than that of Mg_2Sn. However, the present simulation utilizes the parameters from separate simulations of AZ91 alloy [5] and Mg-Sn alloys. The results will be clarified by the ongoing TEM work to investigate

how Al could promote the precipitation of Sn in the ternary alloys. In addition, by using the microstructure evolution information, such as particle size distribution, number density and solute concentration in (Mg) as input, the precipitation hardening and solid solution hardening could be predicted from empirical equations. Thus, the yield strength is obtained and the hardness could also be deduced from the relationship between yield strength and hardness.

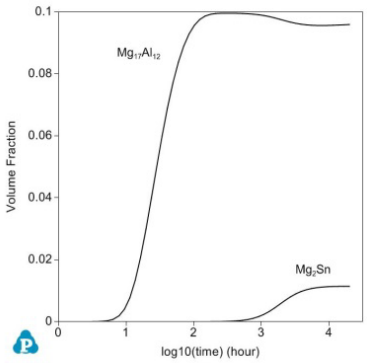

Figure 5. Predicted volume fraction of $Mg_{17}Al_{12}$ and Mg_2Sn precipitates in Mg-7Al-2Sn (wt.%) alloy at 200°C.

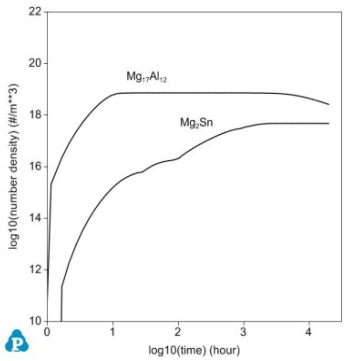

Figure 6. Predicted number density of $Mg_{17}Al_{12}$ and Mg_2Sn precipitates in Mg-7Al-2Sn (wt.%) alloy at 200°C.

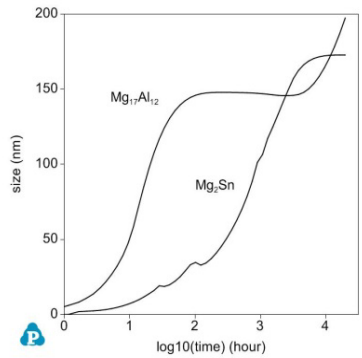

Figure 7. Predicted average size of $Mg_{17}Al_{12}$ and Mg_2Sn precipitates in Mg-7Al-2Sn (wt.%) alloy at 200°C.

Conclusions

Using CALPHAD approach, the atomic mobility parameters of Mg-Al-Sn system are established based on assessment of literature experimental data. By coupling to thermodynamic and atomic mobility parameters, the microstructure evolution in the aging process of two Mg-Sn alloys and concurrent precipitation of $Mg_{17}Al_{12}$ and Mg_2Sn in Mg-7Al-Sn (wt.%) alloy are simulated. It is predicted that the precipitation of $Mg_{17}Al_{12}$ is much strong than that of Mg_2Sn.

Acknowledgements

This work is sponsored by the U.S. Department of Energy under project DE-EE0006450.

References

1. A.A Luo, “Recent magnesium alloy development for elevated temperature applications”, *Int. Mater. Rev.*, 49(1) (2004) 13-30.
2. A.A Luo et al., “Solidification microstructure and mechanical properties of cast magnesium-aluminum-tin alloys”, *Metall. Mater. Trans A.*, 43(1) (2012), 360-368.
3. X.Y. Shi et al., “Microstructure and mechanical properties of Mg-7Al-2Sn alloy processed by super vacuum die-casting”, *Metall. Mater. Trans A.*, 44(10) (2013), 4788-4799.
4. W. Ke et al., “Investigations in the magnesium-tin system”, *Mater. Sci. Forum*, 488-489 (2005), 135-138.
5. C. Zhang et al., “Precipitation simulation of AZ91 alloy”, *JOM*, 66(3) (2014), 389-396.
6. W. Cao et al., “PANDAT software with PanEngine, PanOptimizer and PanPrecipitation for multi-component phase diagram calculation and materials property simulation”, *CALPHAD*, 33(2) (2009), 328-342.
7. PanMagnesium thermodynamic database (Madison, WI: CompuTherm LLC)
8. N. Saunders and A.P. Miodownik, *CALPHAD (Calculation of Phase Diagrams): A Comprehensive Guide* (Elsevier, 1998)
9. J.O. Andersson and J.Ågren, “Models for numerical treatment of multicomponent diffusion in simple phases”, *J. Appl. Phys.*, 72(4) (1992), 1350-1354.
10. B. Jönsson, “Assessment of the mobility of carbon in fcc C-Cr- Fe-Ni alloys”, *Z.Metallkd.*, 85(7) (1994), 502-509.
11. O. Redlich and A.T. Kister, “Algebraic representation of thermodynamic properties and the classification of solution”, *Ind. Eng. Chem*. Res. 40(2) (1948) 345-349.
12. R. Kampmann and R. Wagner, “Kinetics of precipitation in metastable binary alloys-theory and application to Cu-1.9 at % Ti and Ni-14 at % Al”, *Decomposition of Alloys: the early stages, Proceedings of the 2nd Acta-Scripta Metallurgica Conference*, ed. P. Haasen et al. (Pergamon Press, 1983), 91-103.
13. J.E. Morral and G.R. Purdy, “Particle coarsening in binary and multicomponent alloys”, *Scripta Metall. Mater.*, 30(7) (1994), 905-908.
14. P.G. Shewmon, “Self-diffusion in magnesium single crystals”, *Trans. Metall. Soc, AIME*, 206 (1956), 918-922.
15. J. Combronde and G. Brebec, “Anisotropy for self diffusion in magnesium”, *Acta Metall.*, 19(12) (1971), 1393-1399.
16. S. Brennan et al., “Aluminum impurity diffusion in magnesium”, *J. Phase Equilib. Diff.*, 33(2) (2012), 121-125.
17. S.K. Das et al, “Anisotropic diffusion behavior of Al in Mg: diffusion couple study using Mg single crystal”, *Metall. Mater. Trans A.*, 44(6) (2013), 2539-2547.
18. C. Kammerer et al., “Al and Zn impurity diffusion in binary and ternary magnesium solid-solutions,” *Magnesium Technology 2014*, ed. M. Alderman et al., TMS, 2014, 407-411.

19. C. Kammerer et al., “Impurity diffusion coefficients of Al and Zn in Mg determined from solid-to-solid diffusion couples”, *Magnesium Technology 2014*, ed. M. Alderman et al., TMS, 2014, 505-509.
20. S. Brennan et al., “Interdiffusion in the Mg-Al system and intrinsic diffusion in β-Mg_2Al_3”, *Metall. Mater. Trans. A*, 43(11) (2012), 4043-4052.
21. K.N. Kulkarni and A.A. Luo, “Interdiffusion and phase growth kinetics in magnesium-aluminum binary system”, *J. Phase Equilib. Diff.*, 34(2) (2013), 104-115.
22. J. Combronde and G. Brebec, “Diffusion of Ag, Cd, In, Sn and Sb in magnesium”, *Acta Metall.*, 20 (1972), 37-44.
23. Y.W. Cui et al., “Study of diffusion mobility of Al−Zn solid solution”, *J. Phase Equilib. Diff.*, 27(4) (2006), 333-342.
24. John Askill, *Tracer diffusion data for metals, alloys, and simple oxides* (New York, NY, Plenum Publishing Corporation, 1970), 19-26.
25. C. Yu et al., “Ab initio calculation of the properties and pressure induced transition of Sn,” *Solid State Commun.*, 140(11-12) (2006), 538-543.
26. C.L. Mendis et al., “Refinement of precipitate distributions in an age-hardenable Mg-Sn alloy through microalloying”, *Phil. Mag. Let.*, 86(7) (2006), 443-456.